Laminar free-convection from spherical segments

J. Cieśliński and W. Pudlik
Technical University of Gdańsk, ul. Majakowskiego 11/12,
90-952 Gdańsk, Poland

Received October 1986 and accepted for publication July 1987

An experimental investigation of laminar free-convection heat transfer from heated, isothermal, spherical segments to a high Prandtl number liquid is reported. The effect of an extended insulator base on heat transfer is estimated. The experimentally obtained results are compared with theoretically predicted data.

Keywords: free-convection; laminar flow; spherical segments

Heat transfer from the liquid to coal grains floating on the surface of liquid slag has been found to be a decisive factor in the process of gasification of coal by high-temperature combustion products from an MHD generator[1]. This heat transfer takes place under conditions of pure conduction or free convection, the latter being illustrated in Figure 1(a) with a spherical segment representing the immersed part of the floating sphere. The heat transfer coefficients for such a case are not yet known. This prompted investigation of a reversed and enlarged model (Figure 1(b)) with a spherical segment that was heated rather than cooled, because the latter problem appeared to be experimentally difficult to tackle.

Although experimental investigations on free-convection heat transfer from complete heated spheres have already been published[2-8], only Jaluria and Gebhart[9] have obtained information on heat transfer from parts of spheres, and this only from isothermal hemispherical surfaces to water. However, no data on free convection from spherical segments were available until now. This paper reports the results of an investigation into this particular configuration.

The investigation[10] was performed with isothermal spherical segments situated on flat isolated bases. These bases may be considered the free surface of a liquid in the reversed model of a floating, partly submerged sphere. Both the immersed part of the sphere and that jutting out above the liquid surface are spherical segments.

Experimental rig

The experiments were performed on nine spherical segments, all obtained from the same test sphere. The sphere (Figure 2), 78 mm in diameter, was composed of 10 pure copper segments, each separated by an isolating Teflon spacer 0.2 mm thick. The respective spherical segments were obtained by casting around the experimental sphere an appropriate layer of paraffin wax (Figure 3). Paraffin wax was used because it is a good thermal insulator. All segments except the top one were furnished with small electric heaters. The winding was formed of insulated high-resistance wire with a diameter of 0.2 mm and a resistivity of 2 Ω/m. The wire was coiled on bakelite rings. The gap between the wire and the wall of the segment was filled with a special heat conducting paste.

The surface temperature was measured by copper-constantan thermocouples welded to each of the heated segments. Calibrations were performed at 15°C, 30°C, and 50°C by putting the whole sphere in an ultrathermostat.

The tenth segment, which contained no heating wire, was pierced by the support tube. The support tube was made of Teflon and used to bring the power leads and thermocouple wires into the sphere.

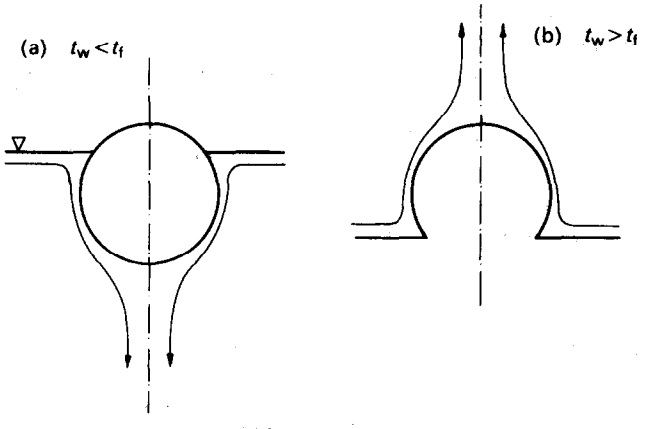

Figure 1 Free-convection flows at (a) a spherical segment heated by the fluid; (b) a spherical segment cooled by the fluid

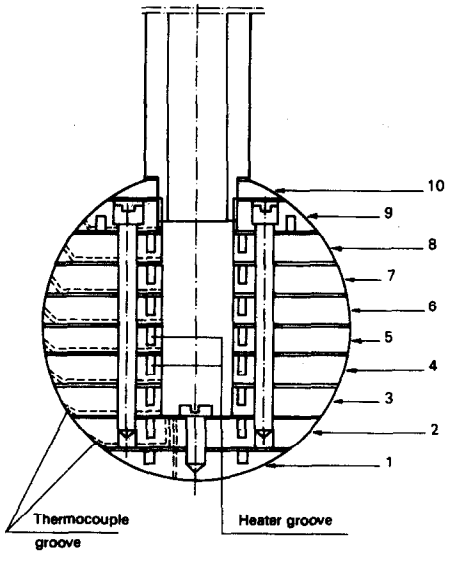

Figure 2 Cross section of the experimental sphere

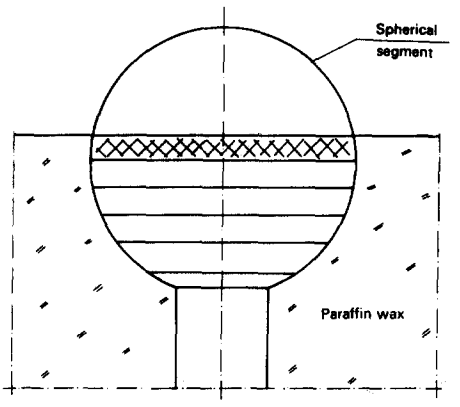

Figure 3 Spherical segment

The spherical segments were immersed during the experiments in glycerine filling a cylindrical, Plexiglass vessel of 300 mm in diameter and 500 mm high. The transparent walls of the vessel enabled us to see the convection currents by using a special visualization technique.

The heaters were each supplied with direct current at a controlled power rate up to 100 W. The power input of each heater was controlled individually by a variac. Voltages and currents were measured individually for each heater by digital voltmeters, from which the power input to each heater was deduced.

Five iron-constantan thermocouples were used to measure the bulk temperature of the fluid at different levels in the vessel.

All thermocouple leads were connected to a rotary switch selector. The results of measurements could also be printed.

The establishing of different steady states was made possible by a cooling system located at the top of the vessel. This system consisted of a copper coil connected to a thermostat.

Experimental procedure

During the experiments a uniform surface temperature of the spherical segments was achieved by adjusting the power input to the individual heaters. The nonuniformity of the temperature measured during all experiments did not exceed 0.2°C.

During the experimental runs the surface temperature of all segments, the bulk temperature of the fluid, and the voltages and currents in the individual heaters were measured. All these data were recorded during established steady states. Steady state was assumed to have been reached when the emf reading varied by less than 3 μV over a 15-min period. The time to establish a steady state was usually about 1.5 h. A higher temperature level was achieved by increasing the voltage and simultaneously lowering the water temperature flowing through the cooling coil. This procedure was repeated until the power level for the particular spherical segment reached its maximum under given operating conditions.

The conduction heat losses from the spherical segments to the supporting tube were eliminated by a counteracting heat flux from an auxiliary heater. By progressive and controlled regulation of the power supply to the auxiliary heater, the temperatures of the spherical segment and of the adjacent segment were balanced, and thus any heat flux was eliminated. The joule heat loss of the lead wires was estimated and taken into account in the total amount of heat supplied to the spherical segment.

The density, thermal expansion coefficient, and dynamic viscosity of the glycerine were experimentally determined. The thermal conductivity of the fluid was taken from published data[11].

The experimental rig was validated by performing a series of experiments with the whole sphere immersed in the liquid. The correlation of the data obtained led to the value $\bar{C}_\varphi = 0.595$, which agrees well with that predicted by the theory presented in the next section as well as with published results of experiments[3–6] and theories[12,13]. This provided evidence that the experimental rig was sound and that the measurement procedure was valid.

Analysis

The theoretical analysis is based on the general method of obtaining approximate solutions of laminar free-convection problems, proposed by Raithby and Hollands[14] and further developed by Chen and Eichhorn[15] for a thermally stratified fluid.

Notation

A	Area
c_p	Specific heat at constant pressure of the fluid
C	Parameter defined by Equation 9
$\bar{C}$	Parameter defined by Equation 11
$\bar{C}_\varphi$	Constant of proportionality between $\overline{\mathrm{Nu}}$ and $(\mathrm{Ra})^{1/4}$
g	Acceleration due to gravity
g_x	Component of gravitational acceleration along a surface
h	Local heat transfer coefficient
$\bar{h}$	Average heat transfer coefficient
k	Thermal conductivity of the fluid
L	Characteristic length
M	Dimensionless ratio defined by Equation 1
$\dot{m}_i$	Mass flow rate in the inner region
$\dot{m}_o$	Mass flow rate in the outer region
$\overline{\mathrm{Nu}}$	Average Nusselt number
$\dot{q}$	Local surface heat flux
R	Radius of a sphere
Ra_L	Rayleigh number based on L
t	Temperature
t_{ch}	Characteristic temperature
t_f	Temperature of the ambient medium
$\bar{t}_i$	Mean temperature in the inner region
t_m	Temperature at point of velocity extremum
$\bar{t}_o$	Mean temperature in the outer region
t_w	Wall temperature
Δt	Wall-to-fluid temperature difference $(t_w - t_f)$
w	Fluid velocity parallel to a surface
x	Coordinate along a surface
y	Coordinate normal to a surface
y_m	y-coordinate at point of velocity extremum
β	Coefficient of thermal expansion of the fluid
δ	Local "conduction thickness"
μ	Dynamic viscosity of the fluid
ρ	Density of the fluid
θ	Angular coordinate
φ	Half central angle of a spherical segment
γ	Quantity defined by Equation 2

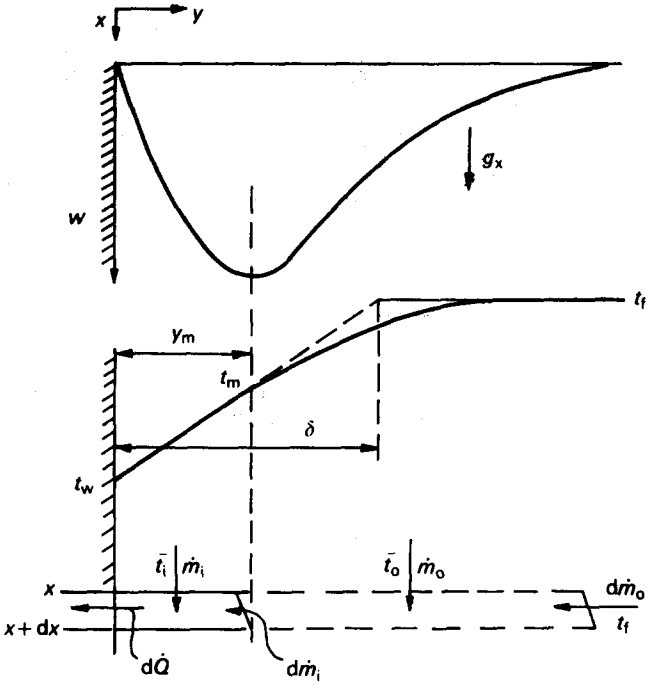

Figure 4 Velocity and temperature profiles for free-convection at a cold wall

The fundamental idea of this method is the division of the boundary layer into the inner region ($y < y_m$, Figure 4) and the outer region ($y > y_m$). The ratio M defined as

$$M = \frac{t_m - t_w}{t_f - t_w} = \frac{y_m}{\delta} \tag{1}$$

indicates the fraction of the total buoyancy taken up by the inner region. According to the authors' hypothesis[14], M and the quantity

$$\gamma \frac{t_f - \bar{t}_o}{t_m - t_w} \tag{2}$$

with

$$\gamma = d\dot{m}_o / d\dot{m}_i \tag{3}$$

may be treated as invariant against x and dependent only on the Prandtl number of the liquid. Having determined the assumed universal dependence of M and $\gamma(t_f - \bar{t}_o)/(t_m - t_w)$ on the Prandtl number, we can calculate the heat transfer rate considering only the inner region.

There is a close analogy between the inner region of a free-convection boundary layer and the liquid film condensation problem. This analogy is brought about by the conductive nature of the heat transfer in both the inner region and the condensate film, and the local balance of viscous and buoyancy forces, which are identical in both cases. By standard Nusselt analysis the following expression for the local heat transfer coefficient is obtained:

$$h = \frac{k}{y_m} M = \frac{k}{\delta(\theta)} \tag{4}$$

With the thermal conductivity of the fluid, k, constant, the heat transfer coefficient can be found from the conduction thickness δ obtained from solving the equations

$$\frac{\partial^2 w}{\partial y^2} = \frac{\rho_f - \rho}{\mu} g_x \tag{5}$$

$$\frac{k(t_m - t_w)}{y_m} dA = d\dot{m}_i c_p (t_f - \bar{t}_i) + d\dot{m}_o c_p (t_f - \bar{t}_o) \tag{6}$$

Equation 5 is the momentum equation for the inner region, and Equation 6 represents the energy balance written for the control volume indicated in Figure 4. For any arbitrary segment of a sphere (Figure 5) the tangential component of the gravitational acceleration is

$$g_x = g \sin(\varphi - \theta) \tag{7}$$

Substituting Equation 7 into 5 and solving Equations 5 and 6 lead to an expression for δ for any arbitrary segment of a sphere:

$$\delta(\theta) = \frac{R\theta}{C(\mathrm{Ra}_{R\theta})^{0.25}} \frac{((1/\theta)\int_0^\theta \sin^{5/3}(\varphi - \theta)\, d\theta)^{0.25}}{\sin^{2/3}(\varphi - \theta)} \tag{8}$$

where

$$C = 0.48[\mathrm{Pr}/(0.861 + \mathrm{Pr})]^{1/4} \tag{9}$$

Substituting Equation 8 into 4 and integrating over the whole surface of a spherical segment give a formula for the average heat transfer coefficient:

$$\bar{h} = k\bar{C}(\mathrm{Ra}_L)^{1/4} \frac{((1/\varphi)\int_0^\varphi \sin^{5/3}(\varphi - \theta)\, d\theta)^{3/4}}{R\int_0^\varphi \sin(\varphi - \theta)\, d\theta} \tag{10}$$

with

$$\bar{C} = \tfrac{4}{3} C \tag{11}$$

Equation 10 may be expressed in terms of a mean Nusselt number:

$$\overline{\mathrm{Nu}} = \bar{C}_\varphi (\mathrm{Ra}_L)^{1/4} \tag{12}$$

The constant $\bar{C}_\varphi$ in Equation 12 is

$$\bar{C}_\varphi = \bar{C} \frac{((1/\varphi)\int_0^\varphi \sin^{5/3}(\varphi - \theta)\, d\theta)^{3/4}}{(1/\varphi)\int_0^\varphi \sin(\varphi - \theta)\, d\theta} \tag{13}$$

As the characteristic length, the surface length in the flow direction is assumed[16] to be

$$L = R\varphi \tag{14}$$

For the whole sphere this theory predicts a value of the constant of

$$\bar{C}_\varphi = 0.5[\mathrm{Pr}/(0.861 + \mathrm{Pr})]^{1/4} \tag{15}$$

Results and Discussion

Figure 6 shows typical experimental results obtained for a hemisphere, where $\overline{\mathrm{Nu}}$ versus Ra is plotted logarithmically. The correlating line was plotted with a slope usually associated with laminar heat transfer, i.e., according to the exponent 0.25

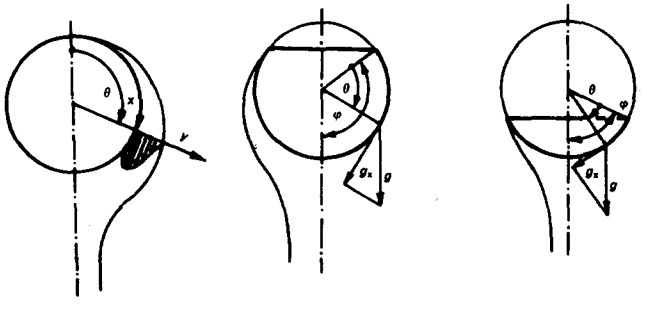

Figure 5 Symbols used for convection at a sphere and at spherical segments

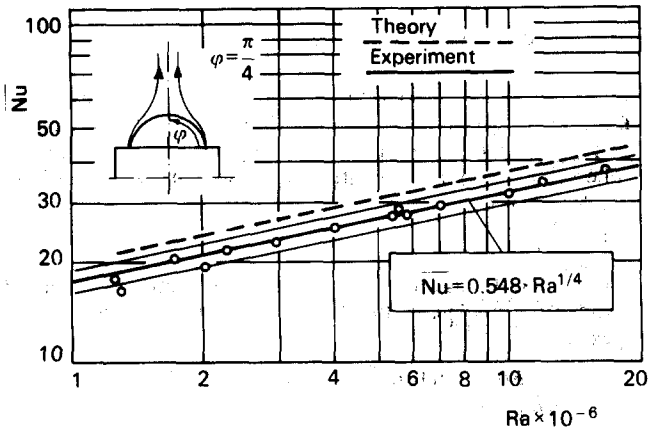

Figure 6 Experimental and theoretical results for the hemisphere

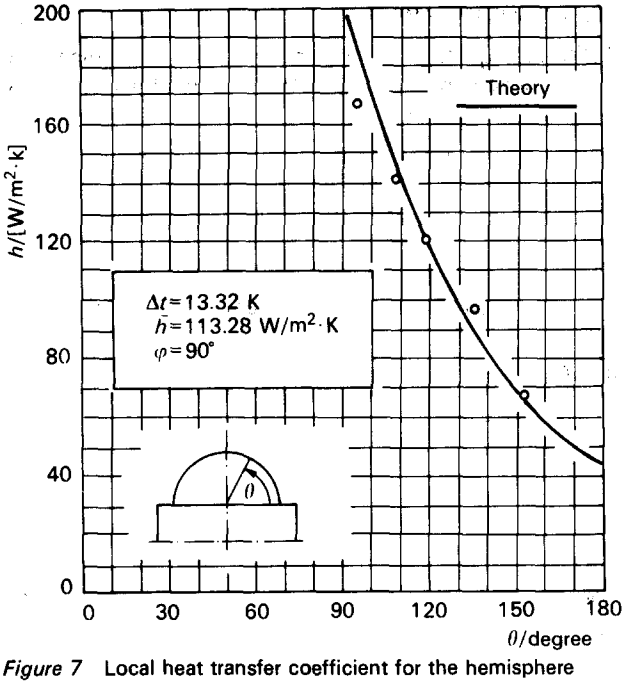

Figure 7 Local heat transfer coefficient for the hemisphere

for the Rayleigh number[16]. The dashed line presents the theoretical solution obtained from numerical integration of Equation 13 by putting $\varphi=\pi/2$. The difference between these lines may be attributed to the presence of the flat base, ignored in the theoretical considerations.

The heat transfer rates, both local and overall, were determined directly from the energy input to the heaters and from the measured wall-to-fluid temperature difference for the individual segment. The heat transfer coefficient is $h=\dot{q}/\Delta t$, where $\dot{q}$ is the local heat flux density calculated from the power input to the individual heater and the area of the outer surface of the individual segment. Correspondingly, $\bar{h}$ is based on the total input to all heaters and the total surface area of the whole spherical segment.

The distribution of local values of h along the perimeter of the hemisphere can be seen in Figure 7. In spite of inaccuracies that may have been caused by transverse temperature gradients between adjacent segments, the experimental results obtained are in fairly good agreement with the theoretical curve. This agreement obviously breaks off at $\theta\cong 150°$, where according to visual measurements the boundary layer separates from the surface and the plume begins. Unfortunately, no measurements could be carried out for $\theta>150°$.

Figure 8 shows the variation of the average heat transfer coefficient $\bar{h}$ versus the size of the spherical segment, characterized by the angle φ. The points along both curves have been obtained from experimental results, indicated in Figure 9, recounted at assumed constant values of temperature differences Δt and constant characteristic temperature t_{ch}. The latter were equal to the arithmetic means of the wall temperatures of the respective spherical segments and of the bulk temperature of the fluid. The values of $\bar{h}$ increase with diminishing sizes of the segment. The highest values, obtained for the smallest, last spherical segment, are in good agreement with results published by Al-Arabi and El-Riedy[17] on a horizontal flat plate.

On the other hand, when φ increases, finally reaching 180°, the correlation curve leads to values that are lower (by 8%) than those measured on a complete sphere placed at a larger distance from the flat base (free sphere). This gives evidence of the influence of the flat base on the heat transfer.

This influence is more pronounced in Figure 9, where results obtained for all spherical segments are plotted as $\bar{C}_\varphi$ against φ. Here the right part of the correlation curve follows the course of the theoretical curve, but at a specified distance, and the result obtained on the free sphere coincides precisely with the theoretical value. The influence of the flat base depends on a reverse component of the velocity vector of the onsetting horizontal fluid stream at the base. This reverse vector retards the boundary layer flow and enlarges the thickness of the boundary layer, which has been confirmed by visualization techniques.

For smaller spherical segments the experimental relationship changes its character and reveals strong disagreement with the theoretical curve. This is caused by the overwhelming influence of the plume above the heated surface. According to the

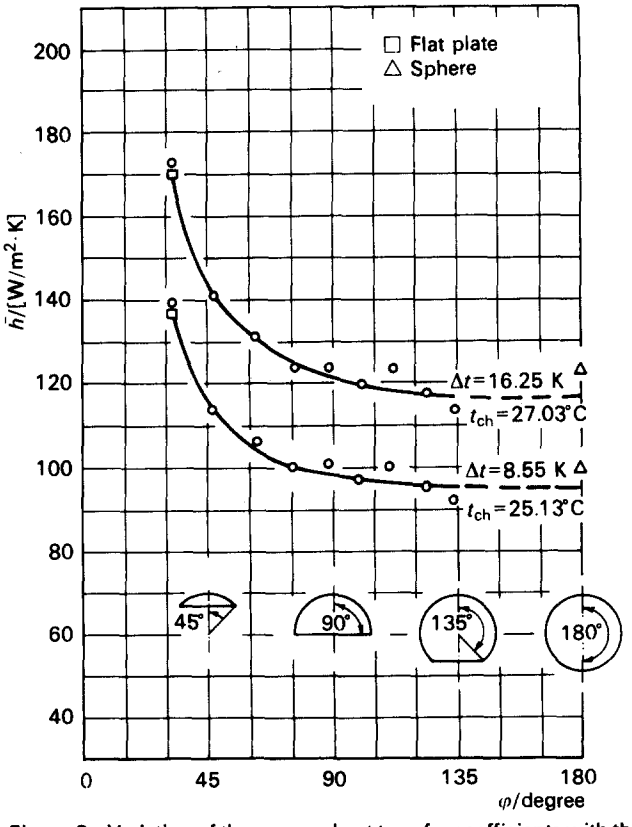

Figure 8 Variation of the average heat transfer coefficients with the size of the spherical segment at constant Δt

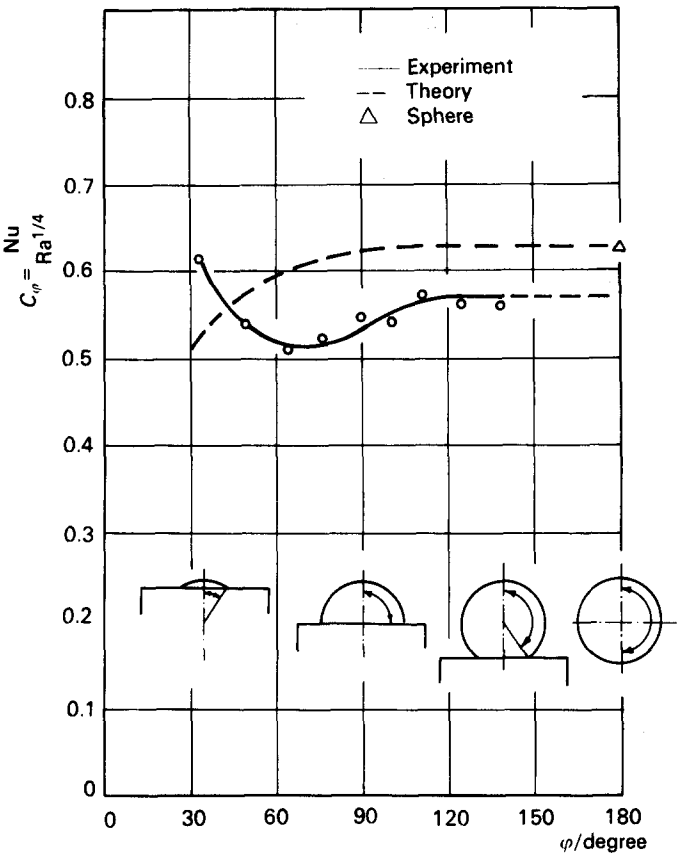

Figure 9 Correlation constant $\bar{C}_\varphi$ from measurements and calculated by the theory as function of the size of the segment

visualization measurements, the plume starts at $\varphi \cong 65°$ in all sizes of investigated spherical segments. The experimental curve in Figure 9, obtained by the least-squares method, reveals a minimum at $\varphi \cong 65°$, which may be attributed to the maximum thickness of the laminar boundary layer just before separation and formation of the plume.

For practical applications the results obtained may be correlated by the formula

$$\overline{Nu} = \bar{C}_\varphi (Ra_L)^{1/4} \tag{16}$$

with

$$\bar{C}_\varphi = 1.011 - 0.01758\varphi + (1.977 \times 10^{-4})\varphi^2 - (6.792 \times 10^{-7})\varphi^3 \tag{17}$$

This formula is valid for $680 < Pr < 1700$ and was obtained at wall temperatures $19.78 < t_w < 44.85$°C and wall-to-fluid temperature differences $4.03 < \Delta t < 28.63$ K.

Conclusions

The laminar free-convection heat transfer from isothermal spherical segments to glycerine may be described by the well-known correlation

$$\overline{Nu} = \bar{C}_\varphi (Ra_L)^{1/4}$$

with values of $\bar{C}_\varphi$ related to spherical segments according to Equation 16.

The theoretical equations of Raithby and Hollands may be used only for larger spherical segments defined by $\varphi > 65°$, when the heat transfer is controlled by the laminar boundary layer; however, a correction factor of about 0.88 regarding the influence of the flat base must be applied.

References

1 Pudlik, W., Stasiek, J., Rogowski, M., and Cieśliński, J. Experiments with gasification of ground coal by outlet gases from the MHD generator, Proc. 8th Int. Conf. on MHD Electrical Power Generation, Moscow, 1983

2 Yuge, T. Experiments on heat transfer from spheres including combined natural and forced convection. *J. Heat Transfer*, 1960, **80C**, 214–220

3 Bromham, R. and Mayhew, Y. Free convection from a sphere in air. *Int. J. Heat Mass Transfer*, 1962, **5**, 83–84

4 Amato, W. S. and Chi Tien. Free convection heat transfer from isothermal spheres in water. *Int. J. Heat Mass Transfer*, 1972, **15**, 327–339

5 Amato, W. S. and Chi Tien. Free convection heat transfer from isothermal spheres in polymer solutions. *Int. J. Heat Mass Transfer*, 1976, **19**, 1257–1266

6 Liew, K. S. and Adelman, M. Laminar natural heat transfer from isothermal sphere to non-Newtonian fluids. *Can. J. Chem. Eng.*, 1975, **53**, 494–499

7 Boberg, J. E. and Starret, P. S. Determination of free convection heat transfer properties of fluids. *Ind. Engng. Chem.*, 1958, **50**, 807–810

8 Cremers, C. J. and Finley, D. L. Natural convection about isothermal spheres. IV Int. Heat Conference, NC 1.5, IV, pp. 1–11, Paris–Versailles, 1970.

9 Jaluria, Y. and Gebhart, B. On the buoyancy-induced flow arising from a heated hemisphere. *Int. J. Heat Mass Transfer*, 1975, **18**, 415–431

10 Cieśliński, J. Badania przejmowania ciepła od kuli i jej odcinków do cieczy o dużej liczbie Prandtla w warunkach laminarnej konwekcji swobodnej [Investigations of laminar natural heat transfer from a sphere and its segments to a fluid having a large Prandtl number]. Ph.D. Dissertation, Gdańsk, 1986

11 Vedhanayagam, M., Lienhard, J. H., and Eichhorn, R. Method for visualizing high Prandtl number heat convection. *Trans. ASME, J. Heat Transfer*, 1979, **101C**, 571–573

12 Merk, H. J. and Prins, J. A. Thermal convection in laminar boundary layer. III. *Appl. Sci. Res.*, 1954, **4A**, 207–221

13 Acrivos, A. Theoretical analysis of laminar natural convection heat transfer to non-Newtonian fluids. *AIChE J.*, 1960, **6**, 584–590

14 Raithby, G. D. and Hollands, K. G. T. A general method of obtaining approximate solutions to laminar and turbulent free convection problems. In *Advances in Heat Transfer*, Vol. 11, Academic Press, 1975, 266–315

15 Chen, C. C. and Eichhorn, R. Natural convection from spheres and cylinders immersed in thermally stratified fluids. *Trans. ASME, J. Heat Transfer*, 1979, **101C**, 566–569

16 Lienhard, J. H. On the commonality of equation for natural convection from immersed bodies. *Int. J. Heat Mass Transfer*, 1973, **16**, 2121–2123

17 Al-Arabi and El-Riedy, M. K. Natural convection heat transfer from isothermal horizontal plates of different shapes. *Int. J. Heat Mass Transfer*, 1976, **19**, 1399–1404